JACS
JOURNAL OF THE AMERICAN CHEMICAL SOCIETY
Communication
pubs.acs.org/JACS

Elucidating the Domain Structure of the Cobalt Oxide Water Splitting Catalyst by X-ray Pair Distribution Function Analysis

Pingwu Du,[†] Oleksandr Kokhan,[†] Karena W. Chapman,[‡] Peter J. Chupas,[‡] and David M. Tiede*[,†]

[†]Chemical Sciences and Engineering Division and [‡]X-ray Science Division, Advanced Photon Source, Argonne National Laboratory, Argonne, Illinois 60439, United States

Supporting Information

ABSTRACT: Pair distribution function (PDF) analysis was applied for structural characterization of the cobalt oxide water-splitting catalyst films using high energy X-ray scattering. The catalyst was found to be composed of domains consistent with a cobalt dioxide lattice sheet structure, possibly containing a Co_4O_4 cubane-type "defect". The analysis identifies the film to consist of domains composed of 13−14 cobalt atoms with distorted coordination geometries that can be modeled by alteration in terminal oxygen atom positions at the domain edge. Phosphate is seen as a disordered component in the films. This work establishes an approach that can be applied to study the structure of in situ cobalt oxide water-splitting film under functional catalytic conditions.

The development of efficient solar-driven water-splitting systems for hydrogen or other fuel production is a central scientific and technological challenge.[1−3] The water oxidation half reaction requires a four-electron transfer process coupled to the removal of four protons from water molecules to form oxygen−oxygen bond, and is considered as a key obstacle for solar hydrogen production.[4−7] In nature, water oxidation occurs in Photosystem II (PS II), containing a $CaMn_4O_4$ cluster as the active site.[4,8,9] To mimic the function of PS II, a variety of oxygen evolution catalysts (OECs) based on manganese clusters have been studied.[4,10,11] Recently, an electrodeposited cobalt oxygen evolution catalyst (Co-OEC) has been reported as a possible functional analogue for PS II, serving as catalyst for both electrochemical and solar-driven water splitting.[12−16] The Co-OEC is of interest for fundamental research and holds promise for practical applications in "personalized energy" because of the robustness, benign operating conditions for catalysis (pH 7.0, room temperature), self-healing properties, and elemental abundance.[17]

Local structure and water oxidation mechanism of the Co-OEC film have been investigated using electron paramagnetic resonance (EPR) and X-ray absorption near-edge (XANES), and X-ray absorption fine structure (XAFS) spectroscopies.[18−20] EPR and XANES measurements have found that cobalt in the phosphate containing Co-OEC films exists as a combination of Co(III) and Co(IV) oxidation states.[18−20] Results from XAFS analyses suggest Co-OEC film consists of Co-oxido clusters with CoO_6 octahedra, consistent with small, corner shared Co_4O_4 cubane-type structures.[19,21] However, further analyses favored models consisting of molecular-sized clusters of edge-sharing CoO_6 octahedra,[18] although the dimensions of the edge-sharing CoO_6 was undetermined.

In the present study, we report on the application high energy X-ray scattering and pair distribution function (PDF) analysis for elucidating the domain size and structure of the Co-OEC. The PDF approach provides an important complement to XAFS studies, by recovering the full range of atom−atom distances, including first shell, outer sphere, and longer range distances that are not directly accessible by XAFS.[22−25] Our results show that atom pair correlations persist to about 13 Å. The PDF patterns could be fit with 13−14 cobalt atom lattice domains, composed of edge-sharing CoO_6 octahedra with distorted geometries at the domain edges, and possibly containing a corner-shared CoO_6 octahedral defect. Phosphate is detected as a largely disordered component in the film. This work demonstrates a direct resolution of the full domain structure in the amorphous Co-OEC, and establishes an approach to develop detailed atomic models of structure-based catalytic mechanism.

Co-OEC film on the surface of ITO (indium tin oxide) was prepared by cathodic electrodeposition process in aqueous buffered solution (pH 7.0, 0.1 M potassium phosphate) containing 0.5 mM $Co(NO_3)_2{\cdot}6H_2O$. The applied voltage is 1.34 V vs NHE. After several hours of deposition, the black color film was air-dried and removed from the electrode surface. The sample was loaded either as an aqueous slurry or dry powder into a 1 mm diameter Kapton tube. Data suitable for PDF analysis were collected at the Advanced Photon Source of Argonne National Laboratory at the beamline 11-ID-B. High-energy X-rays (58 keV, λ = 0.2128 Å) were used in combination with an amorphous silicon-based area detector.[26] Further details are supplied in the Supporting Information.

The electron density pair distribution function, $G(r)$, was obtained from the X-ray scattering data as described previously,[26,27] and shown by Figures S1−S4 and methods described in the Supporting Information. Figure 1 shows the PDF data obtained for the Co-OEC ex situ film formed following 2 h of electrolysis and suspended as an aqueous slurry. Equivalent patterns were measured from either dry powders or aqueous slurries. $G(r)$ patterns were unchanged with prolonged, up to 12 h, electrolytic deposition.

The bulk structure of the Co-OEC was verified by refining different models against the PDF data. This comparison showed that structure mainly consists of domains of edge-

Received: April 20, 2012
Published: June 21, 2012

   dx.doi.org/10.1021/ja303826a | J. Am. Chem. Soc. 2012, 134, 11096−11099

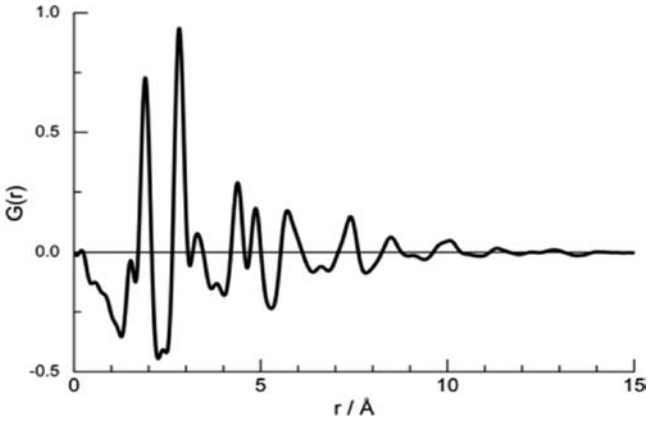

Figure 1. PDF, $G(r)$, measured for a Co-oxide water-splitting catalysts ex situ film.

sharing CoO_6 octahedra within molecular dimensions. Several edge-sharing models with different dimensions were tested. Figure 2 shows the comparison between the experimental $G(r)$

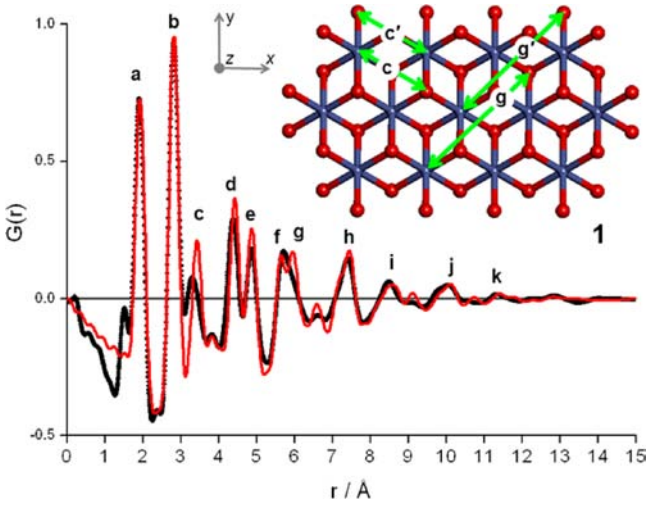

Figure 2. Comparison between the experimental $G(r)$ measured for the Co-oxide catalyst film (black trace) and the $G(r)$ calculated (red trace) from the model structure **1**, inset. Structure **1** was obtained by extracting a 13 Co atom subset from the layered $LiCoO_2$ crystal structure, Inorganic Crystal Structure Database entry 172909-ICSD.[28] Selected peaks in the calculated $G(r)$ are labeled **a**–**k**. The arrows labeled **c** and **c**′ in the inset illustrate representative Co–O atom pairs that contribute to $G(r)$ peak **c**, involving lattice coordinated or terminal oxygen atoms, respectively. Similarly, the arrows labeled **g** and **g**′ in the inset illustrate representative Co–O atom pairs that contribute to $G(r)$ peak **g**, involving lattice coordinated or terminal oxygen atoms, respectively. The calculated $G(r)$ was normalized to the experimental $G(r)$ by the amplitude of the Co–O peak **a**. The *R*-factor between experimental and calculated $G(r)$ in the distance range from 1.7 to 15 Å for model **1** is 0.27.

and one calculated from 13 Co atom model **1**. Overall there is a good correspondence. For example, in the distance range from 1.7 to 15 Å, model **1** has a residue *R*-factor of 0.27 compared to experiment. The 1.7–15 Å distance range covers the ensemble atom pairs in the Co-OEC domains, starting from the first shell Co–O distance, and provides a sensitive measure of the domain size, structure, defect sites, and incorporation of phosphate or other atomic groups into the lattice structure as described below.

Selected peaks in the calculated $G(r)$ are labeled **a**–**k** in Figure 2. Peak **a** corresponds to the first shell Co–O ligand distance, 1.91 Å, and peak **b** corresponds to the 2.82 Å distance between di-μ-oxo/hydroxo-bridged Co atoms. Less strongly weighted O–O pairs also contribute to the 2.82 Å peak. Both of these features are consistent with the observations from XAFS data.[18,19] The longest range pair correlation, peak **k**, not detectable by XAFS, corresponds to the Co–Co distance across four di-μ-oxo/hydroxo-bridges. Peaks in the $G(r)$ can be identified with each of the atom pairs in model **1**, listed in Table S1.

$G(r)$ patterns were found to be sensitive to the size, aspect ratio, and lattice structure of the Co–O domain. Edge-shared models consisting of 12 or fewer Co atoms were found to less accurately fit pair correlations at distances longer than 10 Å, Figures S5, S6. Models composed of corner-shared cubane motifs[18,19] also failed to reproduce the experimental $G(r)$ pattern Figure S7. Edge-shared models consisting of greater than 14 Co atoms fail to match the experimental $G(r)$ peak intensity profile, noticeable with peak **h** and longer distance pairs, Figures S8–S10. While it can be expected that the amorphous Co-OEC will exist as a distribution of domains and sizes, the good correspondence of experiment with single domain 13–14 Co models suggests that the Co-OEC contains a relatively narrow distribution of domain structures, centered on a composition of 13–14 CoO_6 octahedra arranged in an edge-shared lattice. Further modeling studies will need to consider effects of possible distributions of domain size and defects as described below.

Further information on the structure of the Co-OEC domains can be obtained by examining differences between the $G(r)$ calculated for model **1** and the experiment. Most notable are the mismatches occurring between 3–7 Å, corresponding to peaks **c**–**g**. Significant variances are seen for peak **c**, corresponding to Co–O pairs associated with lattice coordinated or terminal O, marked by the arrows **c** and **c**′, respectively, in Figure 2. Similarly, noticeable variances are seen for peak **g**, corresponding to Co–O pairs associated with lattice coordinated or terminal O, marked by arrows **g** and **g**′, respectively, in Figure 2. In model **1**, atom pairs **c** and **c**′ and **g** and **g**′ have identical distances. Selected atom pair refinements can be applied to provide a better fit to experiment.

Model **2** shows a refinement that uniformly shifts the positions of the terminal oxygen atoms by rotating 4° compared to their original positions. This geometry change shortens the **c**′ and **g**′ distances by 0.2 Å. This refinement shifts and broadens peak **c**, and similarly peaks **f** and **g** are merged. This refinement markedly improved the fit to experiment, reducing the residual to 0.19 for **2** in the distance range from 1.7 to 15 Å. Application of random rotational displacement of the terminal oxygen atoms similarly reduced the fit residual by broadening the peaks **c** and **g**, while maintaining a constant Co–O ligand distance, peak **a**.

Distortions to coordination geometries and oxygen atom positions in the lattice could be considered as an alternative to account for the broadening of the $G(r)$ peaks **c** and **g**. However, distortions of this type are constrained by the μ-oxo bridging coordination and the need to preserve the Co–O ligand and Co–Co bis-μ-oxo bridged distances.

Other model refinement concepts were also tested. Of particular interest were models that incorporated a CoO cubane structure within the edge-sharing lattice. For example, a CoO cubane structure was created by adding an octahedral

dx.doi.org/10.1021/ja303826a | J. Am. Chem. Soc. 2012, 134, 11096–11099

cobalt atom to one of the open-faced, Co_3O_4 sites in model **2**. To maintain proper coordination for the bridging oxygen, the CoO cubane formation required deletion of the Co at the adjacent site, resulting in the 13 Co atom model **3**, shown in the inset, Figure 3. Compared to model **2**, the calculated $G(r)$

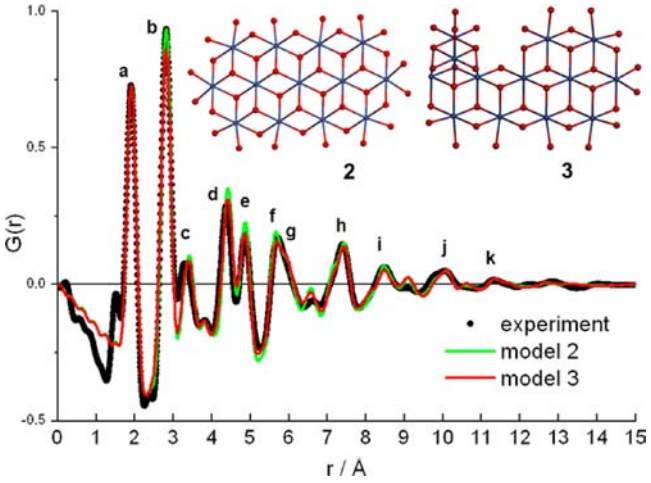

Figure 3. Comparison between the experimental $G(r)$ measured for the Co-oxide catalyst film (black trace) and the $G(r)$ calculated from the model structures **2** (green trace) and **3** (red trace), inset. Structure **2** was derived from **1** by adjusting the positions of terminal O atoms. Structure **3** was derived from **2** by creating a CoO cube defect. Both structures have 13 Co atoms. The *R*-factor difference between experiment and model in the distance range from 1.7 to 15 Å is 0.19 for both structures **2** and **3**.

for **3** provides an equivalent fit to experiment, $R = 0.19$, albeit with different peak correspondences. Notably, model **3** improves the fit to experimental $G(r)$ peaks **c**−**h**. This is offset by an increased variance at peak **b**, occurring because the cubane defect insertion is accompanied by the loss of a di-μ-oxo separated Co−Co pair. In the absence of energetic modeling, the marked improvement in $G(r)$ fitting by models **2** and **3** compared to **1** suggests that geometry distortions for the terminal oxygens and a cubane defect inclusion can both be considered as illustrating candidate distortions of the 13−14 Co atom lattice domain for quantitative modeling of the Co-OEC film.

The effect of phosphate addition to the domain models was also examined. The resulting effect on $G(r)$ varied depending upon whether the phosphate was added as disordered counterions, or as mono-oxo or di-μ-oxo bridged groups. The inclusion of phosphate as disordered counterion added no new features to the $G(r)$ pattern in the 1.7−15 Å distance range. The phosphate P−O pair provided a fit to the 1.5 Å $G(r)$ peak while the relatively weak phosphate O−O makes a minor contribution at 2.4 Å .

The inclusion of phosphate as either oxo or di-μ-oxo bridged groups added characteristic features to the $G(r)$ in the distance range from 1.7 to 15 Å. Bridged phosphate domain models were built using a tetrahedral PO_4 with a 1.5 Å P−O bond distance to coincide with the peak position measured in the experimental $G(r)$. The resulting 2.4 Å O−O atom spacing matches that for the distorted oxygen positions in model **2**. The addition of this group to the domain edge would provide a straightforward mechanism to account for coordination geometry distortions at the terminal oxygen positions. We note that the O−O distances in di-μ-oxo bridged phosphate complexes show considerable variability, ranging from 2.4 to 2.6 Å.[29,30]

Using model **2** as a starting structure, Figures S11 and S12 show a comparison of experimental and calculated $G(r)$ using models that incorporated four di-μ-oxo bridged phosphate groups at different domain edge positions, resulting in residuals compared to experiment that varied from 0.22 to 0.19. In each case, di-μ-oxo bridged phosphate addition produced changes in the $G(r)$ peak **c** shape to more closely fit data, but these improvements were offset by increased deviations in peaks **d**−**k**. The addition of single oxo-bridged phosphate groups to domain models produced a similar, but a weaker impact on the $G(r)$ patterns. For example, Figure S13 shows the $G(r)$ calculated for a model that added four single oxo-bridged phosphates to model **2**. The net residual was unchanged, but variation in individual pair peaks can be seen. To correlate models with the experimental amplitude of the 1.5 Å peak, the number of phosphate groups needed to be increased to approximately 7. For both oxo and di-μ-oxo bridged phosphate models, this addition increased the residuals compared to experiment. For example Figure 4 shows the $G(r)$ calculated for

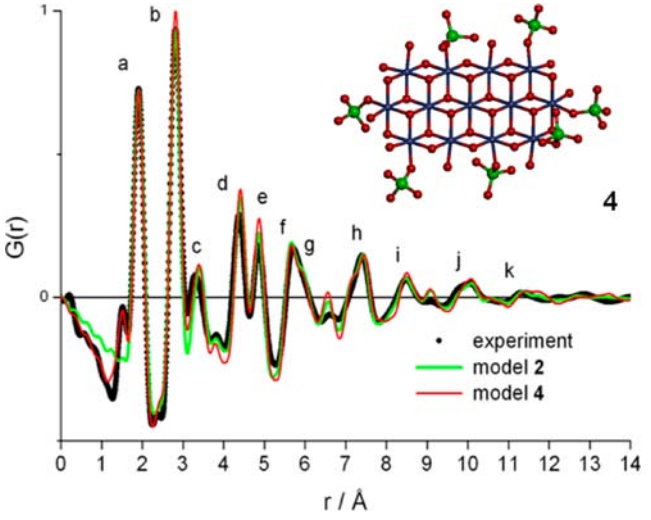

Figure 4. Comparison between the experimental $G(r)$ measured for the Co-oxide catalyst film (black trace) and the $G(r)$ calculated from the model structures **2** (green trace) and **4** (red trace), inset. Structure **4** was derived from **2** by adding seven oxo-linked phosphate groups to arbitrary terminal oxygen positions. The *R*-factor difference between experiment and model in the distance range from 1.7 to 15 Å is 0.19 and 0.20 for structures **2** and **4**, respectively.

structure **4** with 7 oxo-bridged phosphates added to **2**, noticeably adding to individual $G(r)$ peaks, and increasing the residual to 0.2 from 0.19. The effects are greater for di-μ-oxo bridged phosphate addition. These results suggest that if either oxo or di-μ-oxo bridged phosphates are associated with the Co-OEC domain, they must be added as disordered components in order to broaden $G(r)$ contributions to allow a better match to experimental data. The likely disordered nature of phosphate association with the domains fits with recently suggested mechanisms proposed for formation of the Co-OEC film formation, and possible transient, hydrogen-bonded phosphate oxo structures.[31]

The PDF analysis described above suggests that a characteristic feature of the Co-OEC is the distorted coordination

dx.doi.org/10.1021/ja303826a | J. Am. Chem. Soc. 2012, 134, 11096−11099

geometry, which is modeled here for the terminal oxygen atoms at the domain edge positions. This raises the possibility that distorted coordination geometries or defect structures may contribute to the catalytic reactivity. Mechanisms involving a peroxide intermediate have been proposed for water oxidation by the $CaMn_4O_4$ cluster in PS II,[7−9] the ruthenium blue dimer, and the Co-OEC domain.[32,33] The results presented here demonstrate the ability of X-ray PDF measurements to discriminate between candidate structural models for the Co-OEC domain, and suggest opportunities to use PDF data for constrained ab initio structure and catalytic reaction modeling.

■ ASSOCIATED CONTENT

Ⓢ Supporting Information

Experimental details and the fitting data. This material is available free of charge via the Internet at http://pubs.acs.org.

■ AUTHOR INFORMATION

Corresponding Author

tiede@anl.gov

Notes

The authors declare no competing financial interest.

■ ACKNOWLEDGMENTS

This work is supported by the Division of Chemical Sciences, Geosciences, and Biosciences, Office of Basic Energy Sciences of the U.S. Department of Energy under Contract DE-AC02-06CH11357. Use of the Advanced Photon Source, an Office of Science User Facility operated for the U.S. Department of Energy (DOE) Office of Science by Argonne National Laboratory, was supported by the U.S. DOE under Contract No. DE-AC02-06CH11357. P.D. gratefully acknowledges the Director's Fellowship from Argonne National Laboratory.

■ REFERENCES

(1) Lewis, N. S.; Nocera, D. G. *Proc. Natl. Acad. Sci. U.S.A.* **2006**, *103*, 15729−15735.

(2) Esswein, A. J.; Nocera, D. G. *Chem. Rev.* **2007**, *107*, 4022−4047.

(3) Walter, M. G.; Warren, E. L.; McKone, J. R.; Boettcher, S. W.; Mi, Q.; Santori, E. A.; Lewis, N. S. *Chem. Rev.* **2011**, *111*, 5815−5815.

(4) McEvoy, J. P.; Brudvig, G. W. *Chem. Rev.* **2006**, *106*, 4455−4483.

(5) Karlsson, S.; Boixel, J.; Pellegrin, Y.; Blart, E.; Becker, H. C.; Odobel, F.; Hammarstrom, L. *Faraday Discuss.* **2012**, *155*, 233−252.

(6) Eisenberg, R.; Gray, H. B. *Inorg. Chem.* **2008**, *47*, 1697−1699.

(7) Liu, F.; Concepcion, J. J.; Jurss, J. W.; Cardolaccia, T.; Templeton, J. L.; Meyer, T. J. *Inorg. Chem.* **2008**, *47*, 1727−1752.

(8) Umena, Y.; Kawakami, K.; Shen, J.-R.; Kamiya, N. *Nature* **2011**, *473*, 55−60.

(9) Ferreira, K. N.; Iverson, T. M.; Maghlaoui, K.; Barber, J.; Iwata, S. *Science* **2004**, *303*, 1831−1838.

(10) Dismukes, G. C.; Brimblecombe, R.; Felton, G. A. N.; Pryadun, R. S.; Sheats, J. E.; Spiccia, L.; Swiegers, G. F. *Acc. Chem. Res.* **2009**, *42*, 1935−1943.

(11) Tagore, R.; Crabtree, R. H.; Brudvig, G. W. *Inorg. Chem.* **2008**, *47*, 1815−1823.

(12) Cook, T. R.; Dogutan, D. K.; Reece, S. Y.; Surendranath, Y.; Teets, T. S.; Nocera, D. G. *Chem. Rev.* **2010**, *110*, 6474−6502.

(13) Kanan, M. W.; Surendranath, Y.; Nocera, D. G. *Chem. Soc. Rev.* **2009**, *38*, 109−114.

(14) Kanan, M. W.; Nocera, D. G. *Science* **2008**, *321*, 1072−1075.

(15) Pijpers, J. J. H.; Winkler, M. T.; Surendranath, Y.; Buonassisi, T.; Nocera, D. G. *Proc. Natl. Acad. Sci. U.S.A.* **2011**, *108*, 10056−10061.

(16) Swiegers, G. F.; Clegg, J. K.; Stranger, R. *Chem. Sci.* **2011**, *2*, 2254−2262.

(17) Nocera, D. G. *Inorg. Chem.* **2009**, *48*, 10001−10017.

(18) Kanan, M. W.; Yano, J.; Surendranath, Y.; Dinca, M.; Yachandra, V. K.; Nocera, D. G. *J. Am. Chem. Soc.* **2010**, *132*, 13692−13701.

(19) Risch, M.; Khare, V.; Zaharieva, I.; Gerencser, L.; Chernev, P.; Dau, H. *J. Am. Chem. Soc.* **2009**, *131*, 6936−6937.

(20) McAlpin, J. G.; Surendranath, Y.; Dinca, M.; Stich, T. A.; Stoian, S. A.; Casey, W. H.; Nocera, D. G.; Britt, R. D. *J. Am. Chem. Soc.* **2010**, *132*, 6882−6883.

(21) Mattioli, G.; Risch, M.; Bonapasta, A. A.; Dau, H.; Guidoni, L. *Phys. Chem. Chem. Phys* . **2011**, *13*, 15437−15441.

(22) Chupas, P. J.; Chapman, K. W.; Chen, H. L.; Grey, C. P. *Catal. Today* **2009**, *145*, 213−219.

(23) Egami, T.; Billinge, S. J. L. *Underneath the Bragg Peaks: Structural Analysis of Complex Materials*; Pergamon: Amsterdam, 2003; Vol. *7*.

(24) Billinge, S. J. L.; Kanatzidis, M. G. *Chem. Commun.* **2004**, 749−760.

(25) Malavasi, L. *Dalton Trans.* **2011**, *40*, 3777−3788.

(26) Chupas, P. J.; Chapman, K. W.; Lee, P. L. *J. Appl. Crystallogr.* **2007**, *40*, 463−470.

(27) Qiu, X.; Thompson, J. W.; Billinge, S. J. L. *J. Appl. Crystallogr.* **2004**, *37*, 678.

(28) Takahashi, Y.; Kijima, N.; Dokko, K.; Nishizawa, M.; Uchida, I.; Akimoto, J. E. *J. Solid State Chem.* **2007**, *180*, 313−321.

(29) Ichikawa, M. *Acta Crystallogr.* **1987**, *B43*, 23−28.

(30) Hanic, F.; Handlović, M.; Burdová, K.; Majling, J. *J. Chem. Crystallogr.* **1982**, *12*, 99−127.

(31) Surendranath, Y.; Lutterman, D. A.; Liu, Y.; Nocera, D. G. *J. Am. Chem. Soc.* **2012**, *134*, 6326−6336.

(32) Surendranath, Y.; Kanan, M. W.; Nocera, D. G. *J. Am. Chem. Soc.* **2010**, *132*, 16501−16509.

(33) Gerken, J. B.; McAlpin, J. G.; Chen, J. Y. C.; Rigsby, M. L.; Casey, W. H.; Britt, R. D.; Stahl, S. S. *J. Am. Chem. Soc.* **2011**, *133*, 14431−14442.